Enantiomer discrimination illustrated by high-resolution crystal structures of the human nuclear receptor hRARγ

Bruno P. Klaholz*, André Mitschler*, Makonen Belema†, C. Zusi†, and Dino Moras*‡

*Laboratoire de Biologie et Génomique Structurales, Institut de Génétique et de Biologie Moléculaire et Cellulaire, Centre National de la Recherche Scientifique/Institut National de la Santé et de la Recherche Médicale/Université Louis Pasteur, 1, rue Laurent Fries, BP 163, F-67404 Illkirch Cédex, France; and †Pharmaceutical Research Institute, Bristol-Myers Squibb, 5 Research Parkway, Wallingford, CT 06492-7660

The human retinoic acid receptor (hRAR) is a member of the nuclear receptor superfamily that regulates the transcription of target genes in a ligand-dependent manner. The three hRAR isotypes are targets for retinoids that are used in the treatment of various diseases, including breast cancer and skin diseases. Drug efficiency and safety depend on the pharmacological activity of enantiomers, which can differ because of the chiral environment generated by the target. We report the crystal structures of the hRARγ ligand-binding domain bound to two enantiomers, the active BMS270394 and the inactive BMS270395, solved at 1.6 Å and 1.7 Å resolution, respectively. The crystal structures reveal that in both enantiomers, the hydroxyl moiety attached to the chiral center forms a hydrogen bond to the Met-272 sulfur atom, thus imposing a conformation of BMS270395 that differs significantly from that observed for BMS270394 and other known retinoids. BMS270395 adopts an energetically unfavorable conformation, accounting for its inactivity; in contrast, the conformation of BMS270394 is close to an energy minimum. Our high-resolution data allow rationalization of enantiomer discrimination by the receptor and provide a model system for the pharmacological properties of enantiomeric pairs.

T he biological effects of retinoic acids and retinoids in general are mediated through the nuclear receptors (1, 2), retinoid acid receptor (RAR) and retinoid X receptor (RXR), and their α, β, and γ isotypes, which have crucial roles in development, cell differentiation, and homeostasis (3–5). Retinoids are used in the treatment of various skin diseases, including psoriasis and acne, and in the treatment or chemoprevention of cancer, such as acute promyelocytic leukemia, skin, cervical, and breast cancer (refs. 6 and 7 and refs. therein). Numerous synthetic agonist and antagonist retinoids differentiate RXR from RAR or are selective for the RARα, β, or γ isotypes. The different activity of RARγ-specific enantiomers has been described for two retinoids (8, 9). However, the structural reasons for enantiomer discrimination has remained obscure. An initial hint on how such a discrimination may be achieved came from the crystal structure of the hRARγ ligand-binding domain (LBD) complexed with the RARγ-specific agonist BMS189961 (10), a racemic mixture of BMS270394 and BMS270395 (11, 12) (Table 1). Synthesis and characterization of the individual enantiomers (see *Material and Methods*) shows that the biological activity of BMS189961 resides in the *R*-enantiomer (BMS270394), whereas the *S*-enantiomer (BMS270395) shows no measurable binding affinity and transactivation (Table 1). In the following, we describe the crystal structures of the hRARγ LBD bound to BMS270394 and the inactive BMS270395. The high-resolution diffraction data provide details of the enantiomers and the ligand-binding pocket that allow a detailed discussion of the ligand conformation and its effect on ligand activity.

Materials and Methods

Enantiomer Characterization. Synthesis of the racemic BMS189961 follows the synthesis disclosed in European Patent Application no. 747,347. The individual enantiomers were isolated by subjecting the allyl ester of BMS189961 (12) to chiral chromatography (Chiralpak AD column) followed by cleavage of the allyl moiety under mild conditions (morpholine, catalytic palladium: Tetrakis(triphenylphosphine)-palladium). Optical purity was checked by chiral analytical HPLC, after derivatization of the free acid to the corresponding methyl ester. The determination of the absolute configuration was carried out by x-ray crystal analysis of the (R)-Mosher ester of the allyl ester of BMS270394. Details of the enantiomer synthesis and characterization will be published elsewhere.

Protein Crystallization. Purification and crystallization of the hRARγ LBD complexes with BMS270394 and BMS270395 were done by using the described procedure (10, 13, 14). Protein overproduction could be notably improved by addition of 5% sucrose to the cell culture medium. This resulted in a better purification with a subsequent increase of the crystal size. The histidine-tagged hRARγ LBD (domain E) (178–423) was overproduced in an *Escherichia coli*/T7 system and purified by nickel chelate affinity chromatography and gel filtration, before final addition of 2% (volume) of a 20 mM ethanolic ligand solution (1.3 equivalents). Crystallization was carried out at 17°C with the hanging-drop vapor-diffusion method with varying concentrations of NaOAc as a precipitant. Crystals grew within 4–15 days.

Data Collection. The crystals were mounted in fiber loops and flash cooled in liquid ethane or nitrogen after cryoprotection with a mixture containing 15% glycerol and 1.4–1.8 M NaOAc. X-ray diffraction data (Table 3) were collected on a MAR345 detector (Marresearch, Hamburg, Germany) by using single crystals maintained at liquid nitrogen temperature. The diffraction data of the BMS270394 complex were collected at the BW7B beamline at the European Molecular Biology Laboratory, Deutsches Elektronen Synchrotron (Hamburg, Germany). Because of the limited crystal size (see Table 3), the data for the BMS270395 complex were collected first at the ID13 microfocus beamline by using a beam focused to 30 × 30 μm²; the achieved resolution was 2.1 Å. Later, we were able to grow one bigger crystal that allowed extension of the resolution to 1.67 Å at the BM14 beamline of the European Synchrotron Radiation Facil-
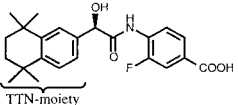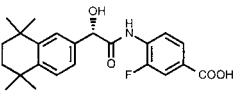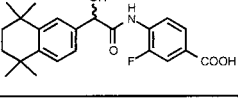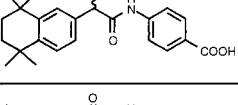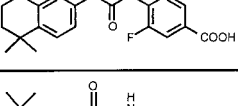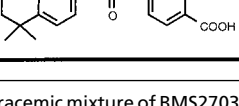
Table 1. Chemical structure and EC$_{50}$ values (nM) of closely related retinoids describing their transcriptional activation properties

Ligand	Formula	RARα	RARβ	RARγ
BMS270394	TTN-moiety	inactive	400	30
BMS270395		inactive	inactive	inactive
BMS189961		inactive	1000	30
BMS187948		>1000	200	20
BMS190914		300	20	20
BMS187949		20	0.8	1

BMS189961 is a racemic mixture of BMS270394 (K_d = 500 nM) and BMS270395 (no binding); the activity resides only in the former. The other ligands show the role of the hydroxyl group and the fluorine atom to generate a RARγ-selective retinoid.

Table 2. Statistics of structure refinement

Ligand complex	BMS270394	BMS270395
Refinement resolution, Å	15–1.59	6–1.67
Observations	37,646	32,478
Residuals		
R_{free}, % (5% of reflections)	25.0	24.3
R_{cryst}, %	20.9	17.9
Model		
Protein atoms	2,167	2,151
Water molecules	327	276
Ligand atoms	29	29
Detergent atoms	35	35
Double conformations	12	11
B_{avg}, Å^2 protein atoms	25.0	23.5
B_{avg}, Å^2 water molecules	43.4	37.8
B_{avg}, Å^2 ligand atoms	17.8	16.7
B_{avg}, Å^2 detergent atoms	47.0	53.5
Stereochemistry		
rmsd bond length, Å	0.012	0.009
rmsd bond angles, °	1.635	2.160
rmsd improper angles, °	0.078	1.451
rmsd dihedral angles, °	25.83	27.27
Ramachandran plot, regions		
Most favored, %	95.1	93.7
Additionally allowed, %	4.9	6.3

Overview of data collection statistics for the ligand complexes of the hRARγ LBD, bound to BMS270394 and BMS270395, respectively. Values in parentheses correspond to the highest-resolution shell. Because of the limited crystal size obtained for the BMS270395 complex, a preliminary data set was collected at the microfocus beamline ID13, ESRF. One further data set was collected on BM14 with the only available bigger crystal. $R_{sym}(I) = \Sigma_{hkl} \Sigma_i |I_{hkl, i} - \langle I_{hkl}\rangle| / \Sigma_{hkl} \Sigma_i |I_{hkl, i}|$, with $\langle I_{hkl}\rangle$ mean intensity of the multiple $I_{hkl, i}$ observations for symmetry-related reflections. rmsd, rms deviation.

ity, Grenoble, France. Data processing was done with DENZO and SCALEPACK from the HKL package (15). The CCP4 package (16) was used for calculations of Wilson plots.

Structure Determination and Refinement. The crystal structure of the different complexes was solved by molecular replacement by using the known structure of the BMS189961 complex as a starting model (10). The preliminary 2.04-Å resolution data set of the BMS270395 complex has been used to solve and refine the structure with CNS 0.4a (17) (R_{free}/R_{cryst} = 28.4%/22.3%) revealing an unexpected ligand conformation. Subsequently, 1.67 Å diffraction data were collected to analyze the BMS270395 complex in more detail. For the two high-resolution data sets, data between 15 Å and 2.0 Å were included in a first rigid body refinement with CNS 0.4a, improving the R_{free}/R_{cryst} values of the model of the BMS270394 (BMS270395) complex from 31/29% (30/28%) to 25/24% (26/25%). A first simulated annealing at T = 500 K (300 K) followed by an individual temperature factor refinement led to an R_{free}/R_{cryst} of 25.5/22.1% (24.4/20.3%); T = 1,000 K led to some side-chain conformations discordant with the electron density maps, resulting in higher R_{free}/R_{cryst} values. The calculated electron density maps [σ_A-weighted 2 F$_{obs}$ − F$_{calc}$ and F$_{obs}$ − F$_{calc}$ maps (18)] allowed placement of the ligand that was subsequently included in the refinement. Building operations included essentially conformational changes of side chains and were carried out with the program O (19). In the following refinement cycles, the resolution was gradually extended to the complete range, and alternate least-square minimization and individual temperature factor refinement were

performed, leading to final values of R_{free}/R_{cryst} 25.0/20.9 (24.3/17.9). All data were included in the refinement (no σ-cutoffs). Multiple conformations were located within σ_A-weighted F$_{obs}$ − F$_{calc}$ electron density maps and refined with CNS. The program SHELXL (20) was used at the end of the refinement of the BMS270395 complex for a better estimate of the respective occupancies of the two ligand conformers. The fluorobenzene moiety between the amide nitrogen atom and the carboxylate moiety of the ligand was refined as two independent copies, whereas the remaining ligand atoms were kept as one copy. A free variable was used to constrain the total occupancy of the two fluorobenzene conformers to 1. Because the bulk solvent correction in SHELXL turned out to be defective, the refinement was done in the resolution range 6–1.67 Å. Backbone superposition of the complexes was achieved by using the LSQ option in O. According to PROCHECK (21), the refined models are better than the average and show no Ramachandran plot outlier (see Table 2). All computations were done on a Compaq Alpha (Digital Unix) OSF1 computer, and Silicon Graphics (Mountain View, CA) stations were used for the graphic operations. The pictures of Figs. 1 and 2 were generated with SETOR (22).

Conformational Analysis. The QUANTA/CHARMM package (23) has been used for the conformational analysis of the free enantiomers starting with the conformation observed in the complex. This included generation of 5,832 ligand conformers (rotation around three dihedral angles by increments of 20°; the carboxylate group and amide moieties were considered rigid; all hydrogens were included in the calculations), energy minimization of each generated conformer with constraints on the dihedral angles, and finally energy calculation. Sections resulting from contours of the calculated energy of each conformer are

Table 3. Data collection statistics

Ligand complex	BMS270394	BMS270395	
X-ray source	BW7B, DESY	ID13, ESRF Microfocus	BM14, ESRF
Wavelength, Å	0.8345	0.6887	0.9612
Approximated crystal size, μm^3	$560 \times 280 \times 280$	$100 \times 60 \times 80$	$200 \times 120 \times 120$
Cell, Å ($\alpha = \beta = \gamma = 90°$)	a = b = 59.67	a = b = 59.90	a = b = 59.85
Space group $P4_12_12$	c = 155.55	c = 154.52	c = 155.62
Resolution, Å	15–1.59	30–2.04	25–1.67
Observed reflections	131,831	46,012	165,142
Unique reflections	37,688	17,279	33,233
Multiplicity	3.50	2.66	4.97
Completeness, %	97.2 (91.2)	92.8 (94.9)	98.2 (97.9)
R_{sym} (I), %	4.4 (30.8)	6.9 (38.3)	3.8 (31.5)
I/σ (I)	27.0 (3.0)	13.5 (2.9)	33.1 (3.5)
Highest resolution shell, Å	1.62–1.59	2.09–2.04	1.70–1.67

Refinement statistics for both enantiomer complexes performed with CNS (17). Because the fluorine atom of BMS270395 was seen in two conformations, final occupancy refinement of the ligand was achieved with SHELXL (20). Double conformations were observed essentially for residue side chains at the protein surface. $R_{cryst} = \Sigma_{hkl}$ | $F_{obs} - F_{calc}$ |/Σ_{hkl} | F_{obs} |. $R_{free} = \Sigma_{hkl\varepsilon\,T}$ | $F_{obs} - F_{calc}$ |/$\Sigma_{hkl\varepsilon\,T}$ | F_{obs} |, the test set T includes 5% of the data (29).

shown in the supplementary material (see www.pnas.org). The values of the dihedral angles (for definition, see supplementary material) of the free ligands in the lowest energy conformation (BMS270394: tor-1/2/3 = 240°/243°/16°; BMS270395: tor-1/2/3 = 156°/132°/336°) compared with those of the bound ligands (BMS270394: tor-1/2/3 = 234°/255°/235°; BMS270395: tor-1/2/3 = 79°/127°/218°) illustrate the ligand adaptation mentioned in *Results and Discussion*.

Results and Discussion

The crystal structures of the RARγ LBD bound to BMS270394 and BMS270395 were determined at 1.59 Å and 1.67 Å, respectively. Both complexes were cocrystallized, and their structure was solved by molecular replacement by using the known hRARγ LBD/BMS189961 structure (10) as a starting model. The crystallographic data are summarized in Tables 2 and 3. Initial omit maps unbiased from the atomic model refinement

have been used to fit the ligands to their electron density, as shown in Figs. 1 and 2A. The high-resolution data allow an accurate description of the geometry of the ligands, revealing the presence of two conformers of BMS270395. Both complexes exhibit a very similar protein structure (rms deviation 0.19 Å on Cα atoms). The side-chains of several residues were refined to precise conformations that differ from those described for the BMS189961 complex. These changes affect in particular Leu-268, Leu-271, Leu-400, and Met-408, which show van der Waals contacts with the ligand.

Structure of the hRARγ LBD/BMS270394 Complex. In the BMS270394 complex, the ligand adopts a conformation similar to that described previously for the BMS189961 complex (10). The carboxylate moiety of the ligand is anchored by a network of hydrogen bonds with Arg-278, Ser-289, a water molecule, and Leu-233 (Fig. 1). The orientation of the hydroxyl group attached
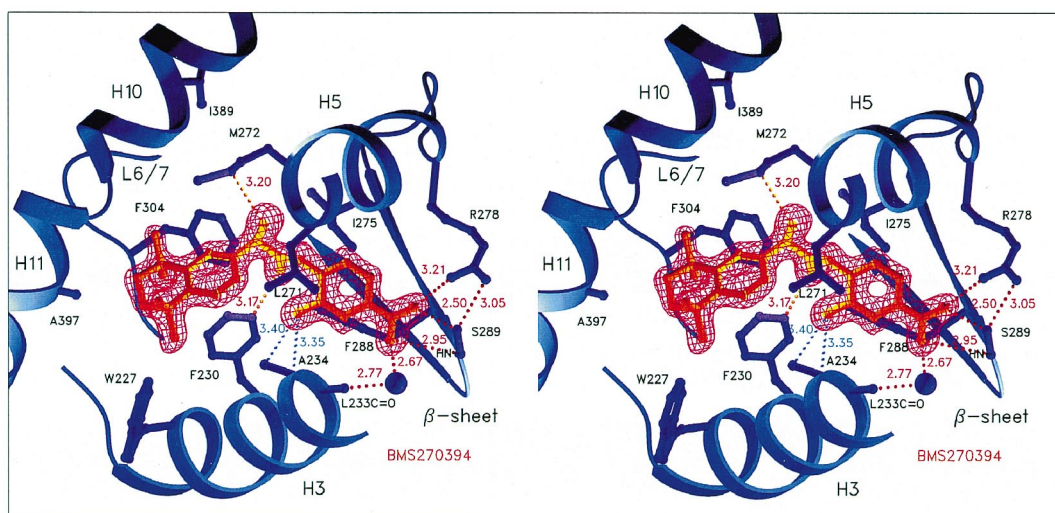

Fig. 1. Stereo representation of the ligand-binding pocket of the crystal structure of the hRARγ LBD with the bound active enantiomer BMS270394 (shown in orange). The final model is depicted with the ligand fitted to the electron density map (colored in red) that has been calculated at the very beginning of the refinement in absence of the ligand. The σ_A-weighted $F_{obs} - F_{calc}$ map (18) at 1.59-Å resolution is contoured at 3.2 σ. Distances in yellow indicate hydrogen bonds and salt bridges between ligand and residues, whereas van der Waals contacts are shown in blue. RARγ selectivity of the ligand is achieved by its hydroxyl group, which forms a hydrogen bond with the sulfur of Met-272, corresponding to isoleucines in RARα and β. H3, H5, H10, and H11 indicate helices, and L6/7 the loop between helix 6 and 7.
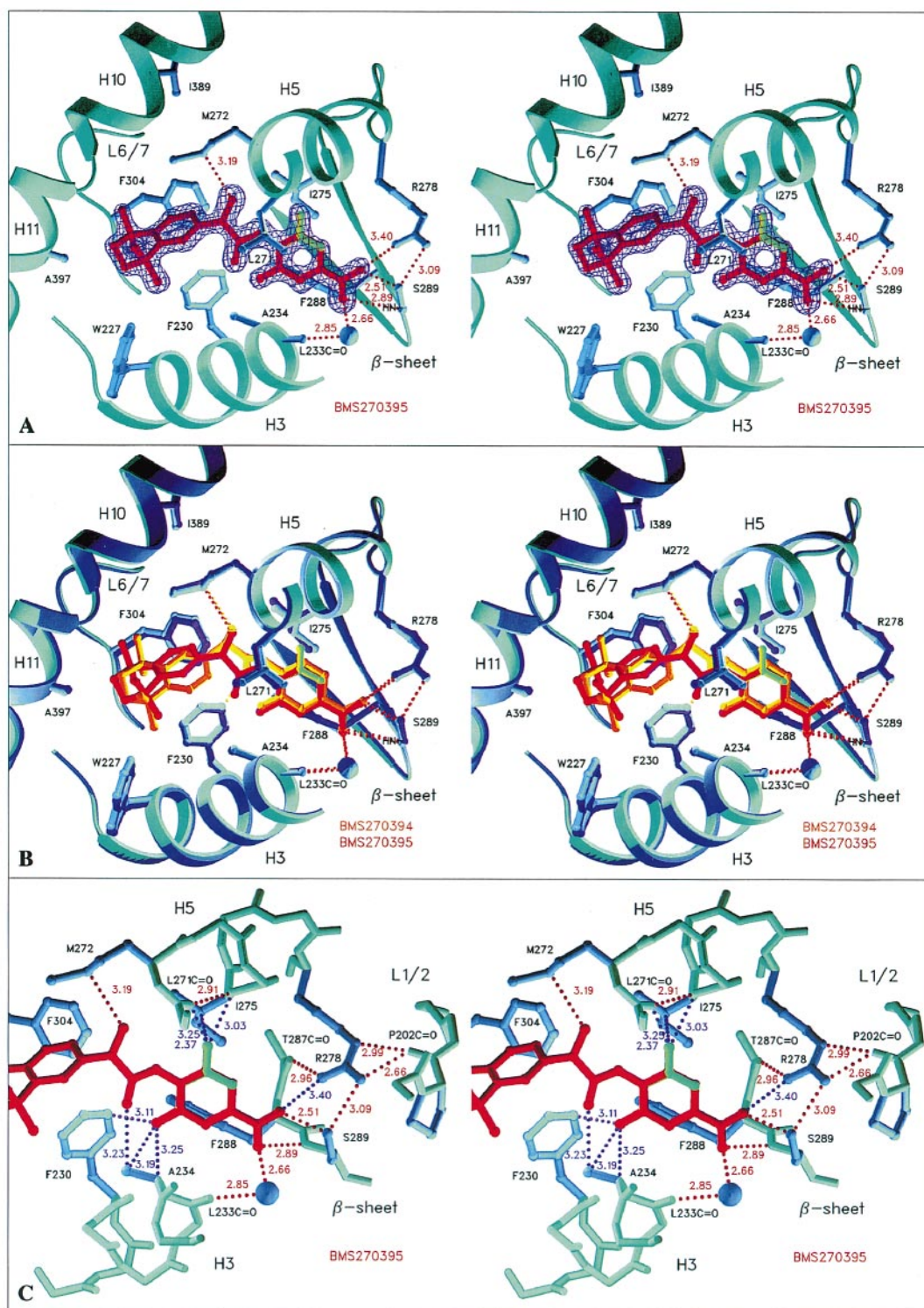
Fig. 2. Structure of hRARγ LBD bound to the inactive BMS270395 and its comparison with the BMS270394 complex (stereo representations) (*A*). The BMS270395 complex with the initial refinement-unbiased σ_A-weighted $F_{obs} - F_{calc}$ map at 1.67 Å resolution contoured at 3.2 σ and colored in violet. The map clearly indicates two possible positions for the fluorine atom, corresponding to two different ligand conformations. The up and down orientations of the fluorine atom have occupancies of 40/60%, respectively (colored in green and red, pointing to Ile-275 and Ala-234, respectively) (*B*). Superposition of the hRARγ LBD complexes of both enantiomers as obtained by a least-squares fit. The position of the hydroxyl group oxygen is strictly conserved to maintain the hydrogen bond to Met-272; BMS270395 therefore adopts a conformation different from that observed for BMS270394 (*C*). Detailed view of the part of the ligand pocket where the ligand exhibits unfavorable contacts. The color code for distances is that of Fig. 1. The fluorine atom exhibits close contacts for both the up and down orientation, whereas the salt bridge between the carboxylate group and Arg-278 is weaker compared with the BMS270394 complex.

at the chiral center in the bridge linking the 5,6,7,8-tetrahydro-5,5,8,8-tetramethyl-2-naphthalenyl (TTN) and the benzoic acid moieties corresponds unambiguously to the *R*-enantiomer of the ligand. Its orientation leads to a good geometry for a hydrogen bond with a distance of 3.20 Å between the oxygen atom of the hydroxyl moiety and the sulfur atom of Met-272. The short distance is an indication of a strong interaction, as suggested by the distances observed between hydroxyl and thioether groups

according to the Cambridge Structural Database (24, 25) (3.2–3.5 Å) and the Protein Data Bank (26) (2.9–3.5 Å).

Two further interactions between the ligand and the receptor are illustrated in Fig. 1. First, the fluorine moiety exhibits short van der Waals contacts with Ala-234 (Cα and Cβ atoms are at 3.35 Å and 3.40 Å, respectively). Second, the oxygen atom of the ligand amide group exhibits a short distance (3.17 Å) to Phe-230. This probably corresponds to a C—H···O hydrogen bond with a

good geometry (the C=O⋯C angle is 131.6°) that may contribute to the stabilization of the complex; similar interactions have been observed in other protein structures (27). Moreover, the nitrogen atom of the amide group forms a hydrogen bond with the backbone carbonyl group of Leu-271 (3.14 Å, not shown).

The basis for the RARγ selectivity is the hydrogen bond between the hydroxyl moiety of BMS270394 and the sulfur atom of Met-272 (Fig. 1) that corresponds to isoleucines in RARα and β (10). Analysis of activation data clearly indicates that the hydroxyl group has an important role in selectivity (Table 1; compare BMS189961 with BMS190914, and BMS187948 with BMS187949, respectively). Substitution of the hydroxyl by a keto group allows no discrimination between RARβ and RARγ (BMS187949 and BMS190914). However, the fluorine atom also contributes to the selectivity, but only if it is combined with the hydroxyl moiety (compare BMS189961 and BMS187948 to BMS190914 and BMS187949, respectively). It allows differentiation between RARβ and -γ probably because of the decreased size of the pocket resulting from the replacement of Ala-397 by a more bulky valine residue in RARβ.

Structure of the hRARγ LBD/BMS270395 Complex.

In contrast to the BMS270394 complex, the crystal structure of the hRARγ LBD bound to the inactive enantiomer (BMS270395) exhibits several unexpected features (Fig. 2A). The hydroxyl group oxygen occupies almost the same position as that of BMS270394 with a similar distance to the Met-272 sulfur atom (3.19 Å), leading to a hydrogen bond with Met-272. However, the superposition of both complexes (Fig. 2B) shows that the TTN moiety has rotated by 98° around the bond linking the TTN and the methylenhydroxyl moieties, leading to a completely different ligand conformation compared with BMS270394. Note that if BMS270395 had adopted the same conformation as BMS270394, there would be enough space in the pocket to accommodate the hydroxyl group with minor adaptations. Thus, the rotation of the TTN moiety and the rearrangement of the amide group occur to maintain both the hydrogen bond to Met-272 and the fit of the TTN moiety.

The electron density map indicates clearly two positions for the fluorine moiety (Fig. 2A) that correspond to two different conformations of the fluorobenzoic acid moiety. In the up orientation, the fluorine atom (40% occupancy) has close contacts with the backbone carbonyl group of Leu-271 (2.37 Å), the nitrogen atom of the backbone amide group (3.03 Å), and Cβ of Ile-275 (3.25 Å) (Fig. 2C). In the down orientation, the fluorine atom (60% occupancy) is closer to the Cα and Cβ atoms of Ala-234 (3.25 Å and 3.19 Å, respectively) than in the BMS270394 complex; it exhibits a short distance to Phe-230 (3.11 Å) and to the oxygen atom of the ligand amide group (2.52 Å, not shown), that is close to the Ala-234 Cβ atom (3.23 Å, Fig. 2C). For both orientations, the observed distances are smaller than those found for similar contacts in the Cambridge Structural Database; in particular, the closest contact between a fluorine and a carboxylate group oxygen corresponds to a distance of 2.75 Å in contrast to the observed 2.37 Å between the fluorine and the backbone carbonyl group of Leu-271. These short distances suggest an increase of the van der Waals repulsion between the protein and the fluorine atom in both positions. The resulting instability may explain the presence of an equilibrium between two conformations. Interestingly, the up and down orientations of the fluorine moiety correspond to the 20-methyl group of all-*trans* and 9-*cis* retinoic acids, respectively, with the difference that the methyl group of the former exhibits good van der Waals contacts (10, 13).

The conformation of BMS270395 and its close contacts with residues in the pocket result in a slight ligand shift toward Ala-397 (helix H11, Fig. 2B). The side chain of Arg-278 cannot compensate this movement because it is involved in a hydrogen

bond network including the backbone carbonyl groups of Pro-202 and Thr-287 and the side-chain hydroxyl group of Ser-289 (Fig. 2C). Therefore, the salt bridge between the ligand's carboxylate group and Arg-278 is weaker than in the BMS270394 complex (distances of 3.40 Å and 3.21 Å, respectively). The small adaptations in the range of 0.5 Å observed for Trp-227, Phe-230, Leu-271, and Phe-201 are not sufficient to avoid the steric contacts of the fluorine atom discussed above.

Conformation of the Enantiomers.

Taken together, the present data suggest that the low affinity and activation capacity of BMS270395 is probably a combined effect of the ligand conformation and the unfavorable contacts of the fluorine moiety with residues of the pocket. A conformational analysis of the free enantiomers corroborates this hypothesis and reveals that BMS270394 exhibits large low-energy wells, in contrast to narrow wells limiting the conformational freedom of BMS270395 (energy contour plots are shown in the supplementary material, www.pnas.org). Importantly, note that this difference is exclusively because of the inversion of the hydroxyl group attached at the chiral center. The conformation of BMS270394 found in the complex is close to an energy minimum of the free ligand. In contrast, BMS270395 adopts a conformation far from an energy minimum in the free state; the energetically unfavorable conformation of this enantiomer disfavors ligand binding and is in accordance with its lack of activity.

The comparison of both enantiomer complexes illustrates a ligand adaptation to the structurally conserved pocket as previously reported for the natural retinoic acids (10). The ligand flexibility depends strongly on the length of the bridge between the TTN and the benzoic acid moieties. Retinoids where the TTN moiety and a naphthoic acid are connected by a single atom (8, 9) have only two rotatable dihedral angles, whereas BMS270395 has three. This flexibility allows the latter to adapt to the pocket and to maintain the hydrogen bond to Met-272.

Receptor Conformation.

Although the different properties of BMS270394 and BMS270395 can now be understood, two questions remain to be answered in relationship with the inactivity of BMS270395: (*i*) how could the crystalline complex be formed, and (*ii*) why are the two complexes isomorphous? Indeed, it is believed that the nuclear receptor activity relies on the ligand-dependent position of the transactivation helix H12 (2, 13), and in both complexes this position corresponds to that expected for an agonist complex. BMS270395 adapts to the agonist pocket without disrupting it, thus preserving all interactions that maintain the position of helix H12. The only difference with the active enantiomer complex is the high energy of the system. This is compensated by the protein and ligand concentrations that favor the association between the receptor and the ligand. Indeed, the protein concentration used for crystallization is approximately 0.1 mM and thereby is in the same range as the affinity of the ligand, as estimated (28) by the conformational energy difference between the active and inactive enantiomers ($\approx$4–5 kcal/mol; therefore, the affinity of BMS270395 is three orders of magnitude lower [estimated: K_d $\approx$0.5 mM] than that of BMS270394 [measured: K_d = 0.5 μM]). This is in contrast with the physiological context and the conditions of transactivation essays. We cannot exclude that the crystallization process may have selected the active conformation of the receptor from different conformations present in solution. However, once the active receptor conformation is adopted, it is unique for different ligands (10), and hence the packing of the molecules in the crystal leads to isomorphous structures.

Discrimination Between Enantiomers.

The present crystal structures explain why all biological activity of the racemic mixture

(BMS189961) resides in BMS270394. In particular, the inactivity of BMS270395 is probably because of its low affinity and not the induction of an inactive receptor conformation. The low affinity can be explained by the unfavorable contacts between the ligand and residues of the pocket and by the energetically unfavorable conformation adopted in the complex. A clear illustration of the discrimination between enantiomers comes from the comparison of the previously reported structure of the BMS189961 (a racemic mixture) complex at 2.5 Å resolution (10) and the now available high-resolution structures of each enantiomer complex. The latter allow an unambiguous assignment of the ligand chirality and confirm that the ligand conformation seen in the BMS189961 complex corresponds to that of the active enantiomer.

The energy contribution of the hydrogen bond between the hydroxyl moiety of the ligands and the Met-272 sulfur atom is important because it allows partial compensation of the energetically unfavorable conformation of BMS270395. It leads to the unexpected result that the position of the oxygen atom of the hydroxyl group is almost conserved in both enantiomer complexes. Moreover, this hydrogen bond is the molecular basis for the RARγ selectivity of BMS270394, enhanced by the presence of the fluorine atom.

BMS270394 and BMS270395 confirm the generally accepted rule that the low-energy conformation of the free ligand should be close to that of the bound one. The conformational analysis reveals that the different orientation of the hydroxyl moiety in the enantiomers leads to a conformational restraint in the case of BMS270395 that allows a ligand adaptation to the structurally conserved pocket (10) only at the expense of an energetically unfavorable conformation. Without the information from the crystal structure, one would not have predicted that BMS270395 binds in a different conformation than other retinoids, and the adopted conformation could not have been forecast. This shows the important role of crystal structure determination for drug design.

The present data provide a model system for enantiomeric pair recognition. Regarding a proposed four-location model for the discrimination between enantiomers (30), the present work shows that the three attachment sites (for the TTN, benzoic acid, and hydroxyl groups) are not sufficient to sterically discriminate one of the two enantiomers. The ligand flexibility allows both enantiomers to bind with different conformations, but with an energy penalty.

The structural investigation of the hRARγ LBD complexes with the separated enantiomers emphasizes the importance of considering enantiomers in early stages of drug development. The administration of an active enantiomer alone can result in a simpler pharmacological profile by reducing side effects, the higher costs that arise from the separation of enantiomers being overcompensated by the drug efficiency and safety in therapeutic use.

1. Mangelsdorf, D. J., Thummel, C., Beato, M., Herrlich, P., Schutz, G., Umesono, K., Blumberg, B., Kastner, P., Mark, M., Chambon, P., *et al*. (1995) *Cell* **83,** 835–839.
2. Moras, D. & Gronemeyer, H. (1998) *Curr. Opin. Cell Biol.* **10,** 384–391.
3. Chambon, P. (1996) *FASEB J.* **10,** 940–954.
4. De Luca, L. M. (1991) *FASEB J.* **5,** 2924–2933.
5. Kastner, P., Mark, M. & Chambon, P. (1995) *Cell* **83,** 859–869.
6. Nagpal, S. & Chandraratna, R. A. S. (1996) *Curr. Pharmacol. Des.* **2,** 295–316.
7. Tallman, M. S. & Wiernik, P. H. (1992) *J. Clin. Pharmacol.* **32,** 868–888.
8. Chen, S., Ostrowski, J., Whiting, G., Roalsvig, T., Hammer, L., Currier, S. J., Honeyman, J., Kwasniewski, B., Yu, K. L., Sterzycki, R., *et al*. (1995) *J. Invest. Dermatol.* **104,** 779–783.
9. Reczek, P. R., Ostrowski, J., Yu, K. L., Chen, S., Hammer, L., Roalsvig, T., Starrett, J. E., Jr., Driscoll, J. P., Whiting, G., Spinazze, P. G., *et al*. (1995) *Skin Pharmacol.* **8,** 292–299.
10. Klaholz, B. P., Renaud, J.-P., Mitschler, A., Zusi, C., Chambon, P., Gronemeyer, H. & Moras, D. (1998) *Nat. Struct. Biol.* **5,** 199–202.
11. Taneja, R., Roy, B., Plassat, J. L., Zusi, C. F., Ostrowski, J., Reczek, P. R. & Chambon, P. (1996) *Proc. Natl. Acad. Sci. USA* **93,** 6197–6202.
12. Swann, R. T., Smith, D., Tramposch, K. M. & Zusi, F. C. (1997) U.S. Patent 5,624,957.
13. Renaud, J.-P., Rochel, N., Ruff, M., Vivat, V., Chambon, P., Gronemeyer, H. & Moras, D. (1995) *Nature (London)* **378,** 681–689.
14. Rochel, N., Renaud, J.-P., Ruff, M., Vivat, V., Granger, F., Bonnier, D., Lerouge, T., Chambon, P., Gronemeyer, H. & Moras, D. (1997) *Biochem. Biophys. Res. Commun.* **230,** 293–296.
15. Otwinowski, Z. & Minor, W. (1997) *Methods Enzymol.* **276,** 307–326.
16. Collaborative Computational Project, No. 4 (1994) *Acta Crystallogr. D* **50,** 760–763.
17. Brünger, A. T., Adams, P. D., Clore, G. M., Delano, W. L., Gros, P., Grosse-Kuntstleve, R. W., Jiang, J. S., Kuszewski, J., Nilges, M., Pannu, N. S., *et al*. (1998) *Acta Crystallogr. D* **54,** 905–921.
18. Read, R. J. (1986) *Acta Crystallogr. A* **42,** 140–149.
19. Jones, T. A., Zou, J. Y., Cowan, S. W. & Kjeldgaard, M. (1991) *Acta Crystallogr. A* **47,** 110–119.
20. Sheldrick, G. M. & Schneider, T. R. (1997) *Methods Enzymol.* **277,** 319–343.
21. Laskowski, R. A., MacArthur, M. W., Moss, D. S. & Thornton, J. M. (1993) *J. Appl. Crystallogr.* **26,** 283–291.
22. Evans, S. V. (1993) *J. Mol. Graphics* **11,** 134–138.
23. Gardner, S. & Thornton, J. (1997) QUANTA (Molecular Simulations, San Diego, CA).
24. Allen, F. H. S. & Watson, D. G. (1979) *Acta Crystallogr. B* **35,** 2331–2339.
25. IDITIS (Oxford Molecular, Oxford), Version 3.0.
26. Bernstein, F. C., Koetzle, T. F., Williams, G. J., Meyer, E. E., Jr., Brice, M. D., Rodgers, J. R., Kennard, O., Shimanouchi, T. & Tasumi, M. (1977) *J. Mol. Biol.* **112,** 535.
27. Wahl, M. C. & Sundaralingam, M. (1997) *Trends Biochem. Sci.* **22,** 97–102.
28. Zhang, T. & Koshland, D. E. (1996) *Protein Sci.* **5,** 348–356.
29. Brünger, A. T. (1992) *Nature (London)* **355,** 472–474.
30. Mesecar, A. D. & Koshland, D. E., Jr. (2000) *Nature (London)* **403,** 614–615.

BIOCHEMISTRY